CHEMICAL ENGINEERING TRANSACTIONS
VOL. 41, 2014
A publication of AIDIC
The Italian Association of Chemical Engineering
www.aidic.it/cet
Guest Editors: Simonetta Palmas, Michele Mascia, Annalisa Vacca
Copyright © 2014, AIDIC Servizi S.r.l.,
ISBN 978-88-95608-32-7; **ISSN** 2283-9216
DOI: 10.3303/CET1441067

Photoelectrochemical Characterization of Hierarchical TiO_2 Nanoarchitectures Obtained by Reactive Pulsed Laser Deposition (PLD)

Roberto Matarrese*[a], Simonetta Palmas[b], Isabella Nova[a], Andrea Li Bassi[c], Carlo S. Casari[c], Valeria Russo[c], Michele Mascia[b], Annalisa Vacca[b]

[a]Laboratory of Catalysis and Catalytic Processes, Dipartimento di Energia, Politecnico di Milano, P.zza L. da Vinci 32, 20133, Milano, Italy
[b]Dipartimento di Ingegneria Meccanica Chimica e dei Materiali, Università degli Studi di Cagliari, Via Marengo 2, 09123 Cagliari, Italy
[b]Micro- and Nanostructured Materials Lab., Dipartimento di Energia, Politecnico di Milano; via Ponzio 34/3, 20133 Milano, Italy
*roberto.matarrese@polimi.it

This work is focused on hierarchical TiO_2 based electrodes prepared by PLD, to be used in the electrically enhanced water splitting process. The photoresponse is analyzed in a range of wavelength of the incident radiation from 365 to 430 nm. Both the capacitive properties of samples and the quantity/accessibility of the existing active sites are examined by means of CV and EIS measurements. The O_2 partial pressure adopted in the PLD synthesis of the samples demonstrated to be the most influential parameter on the final performances of the samples.

1. Introduction

In the field of the photo-electrocatalysis, TiO_2 represents the most widely investigated material and a wide variety of TiO_2 nanostructures have been so far proposed. Nevertheless, some open issues still remain to be addressed to push the material performances up to the technology commercialization, including light management and preferential or channelled charge transport. In this context, the capability to tune material properties such as morphology, structure and oxide phase can be beneficial to understand structure-properties relationship and to design materials with enhanced functionalities.
Using the Pulsed Laser Deposition (PLD) in a background atmosphere, it is possible to produce tree-like hierarchical assemblies, such as quasi 1-D architectures consisting of nanocrystalline TiO_2 particles assembled in nano and mesostructures hierarchically organized at a multiscale level. These systems have already shown their potential in photocatalytic and photovoltaic applications, since they combine large surface area with a multiscale porosity for electrolyte diffusion with light scattering and preferential charge transport along the vertical direction (hybrid or dye-sensitized solar cells) (Di Fonzo et al., 2009; Sauvage et al., 2010; Passoni et al., 2013). However, the optimization of the functional properties of such architectures for water splitting and their relation with the working mechanisms are still open, thus the control of electronic properties and the resulting functionality of these structures represent a point of great interest in view of technological applications.
On these basis, in this work photoelectrochemical characterization techniques (in particular voltammetry and electrochemical impedance spectroscopy) were used to highlight the behaviour of TiO_2 tree-like hierarchically structured films with particular reference to electrochemical surface-related and transport phenomena.

Please cite this article as: Matarrese R., Palmas S., Nova I., Li Bassi A., Casari C., Russo V., Mascia M., Vacca A., 2014, Photoelectrochemical characterization of hierarchical tio2 nanoarchitecures obtained by reactive pulsed laser deposition (pld), Chemical Engineering Transactions, 41, 397-402 DOI: 10.3303/CET1441067

2. Materials and Methods

2.1 Synthesis and morphological characterization of TiO_2 hierarchical photoanodes

TiO_2 hierarchically structured films were deposited, at room temperature, by ablating a TiO_2 target (0.25mm thick, 99.7% metal basis, Aldrich) with UV laser pulses (7ns, 266nm) from a Nd:YAG laser in the presence of a background O_2 gas pressure (in the 5-10Pa range). Films were deposited at a constant mass per unit surface of about 0.15-0.2 mg/cm^2. Further details of sample preparation are reported in previous works (Di Fonzo et al., 2009; Sauvage et al., 2010; Passoni et al., 2013). Post deposition thermal annealing was performed for 2 hours in air in a muffle furnace at 500°C to induce crystalline order.
The morphology of the obtained oxide films was evaluated using a field-emission scanning electron microscope (ZEISS Supra 40 FEG-SEM).

2.2 Photoelectrochemical characterization

A three-electrode cell was used for the photoelectrochemical runs, in which the TiO_2 sample was the working electrode (nominally 1 cm^2), whereas a platinum grid and a saturated calomel (SCE) electrode were the counter and the reference electrodes, respectively. All the values of potential in the text are referred to SCE.
Photo-current tests were performed in 0.1M KOH solution at a constant overpotential of 0.5V versus OCV. The light source was a 300W Xe lamp (Lot Oriel) equipped with an IR water-filter and with suitable optical filters to select the wavelengths 365, 380, 400 and 430nm. Depending on the filter, the average light power incident on the electrode surface ranged from 1.2 to 12.7mWcm^{-2}. For this reason, photocurrents were normalized with respect to the incident light power.
Cyclic voltammetry (CV) measurements were performed in 0.1 M KOH between -0.1 and 0 V with a scan rate ranging from 10 to 100 mVs^{-1}. Voltammetric scans were also performed, with a scan rate of 200 mVs^{-1}, starting from the OCV towards negative potentials down to −1.5 V, then backwards to 0.8 V and again to −1.5 V.
Electrochemical Impedance Spectroscopy (EIS) measurements were performed in 0.1 M KOH, in the frequency range from 100 kHz to 0.1Hz. Measurements were done in the dark at a bias potential at which capacitive behaviour of samples was observed.
A frequency response analyzer (FRA, Model 7200 AMEL) coupled with a potentiostat (AMEL 7050) were employed.

3. Results and discussion

3.1 Photoanode structure and morphology

Figure 1 shows SEM micrographs of films deposited at 5 and 10Pa O_2 after annealing in air at 500°C. A “tree like” hierarchical organization of the film is clearly visible at 10Pa. According to previous results, SEM analyses carried out on samples deposited at different pressure (not shown) pointed out a clear effect of the background pressure on the film morphology. In particular, compact and dense films were obtained by decreasing the background pressure down to 3Pa O_2. At the opposite, at 10Pa O_2, hierarchical structures become more open.
As the same mass was deposited for these samples, the increase in film thickness from about 500nm to ca. 2.6µm moving from 3 to 10Pa O_2 pressure corresponds to a change in the material density (i.e. the density decreases from 3.2 g/cm^3 to about 0.7 g/cm^3).

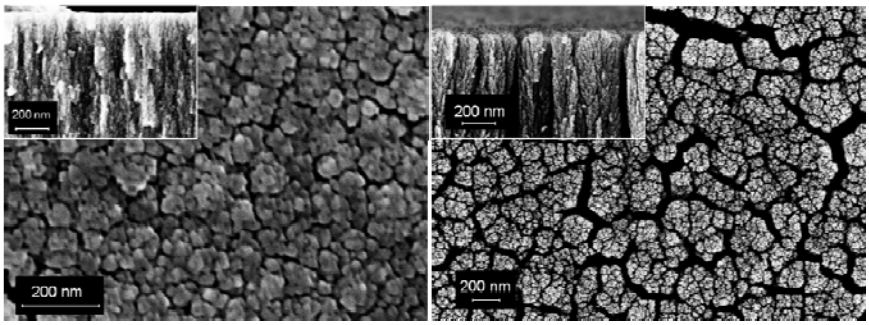

Figure 1: SEM images of samples deposited at 5 Pa (left) and 10 Pa (right) after annealing at 500 °C for 2h.

The estimated porosity (percentage of voids and expressed as the ratio between film density and bulk anatase density (ca. 3.9 g/cm^3)) increased from 18% at 3Pa O_2 to about 83% at 10Pa O_2.
All the as deposited films showed a highly disordered and almost amorphous structure as a result of the room temperature growth process, while, as expected, thermal treatments induce crystallization, as revealed by Raman spectroscopy (not shown). For annealed samples obtained at 3 and 5Pa, no substantial differences in the Raman spectra were observed, and only the presence of the anatase phase was detected; a small fraction of rutile phase was instead observed for films deposited at 10Pa (Di Fonzo et al., 2009).

3.2 Photoelectrochemical characterization

Figure 2A shows the trend of photocurrents, normalized with respect to incident light power, measured at 0.5 V versus OCV and at different wavelengths for the three samples obtained at different O_2 partial pressures. The best efficiencies were obtained in the range of the lower wavelengths, indicating that only the most energetic light is able to activate the generation of charge in the structures of all the samples. In a previous work (Di Fonzo et al., 2009), it was reported that the optical gap for PLD hierarchical TiO_2 systems deposited in O_2 atmosphere and annealed in air at 500°C is about 3.2-3.3 eV, i.e. about 370-390 nm, without any detectable trend with respect to the deposition pressure.

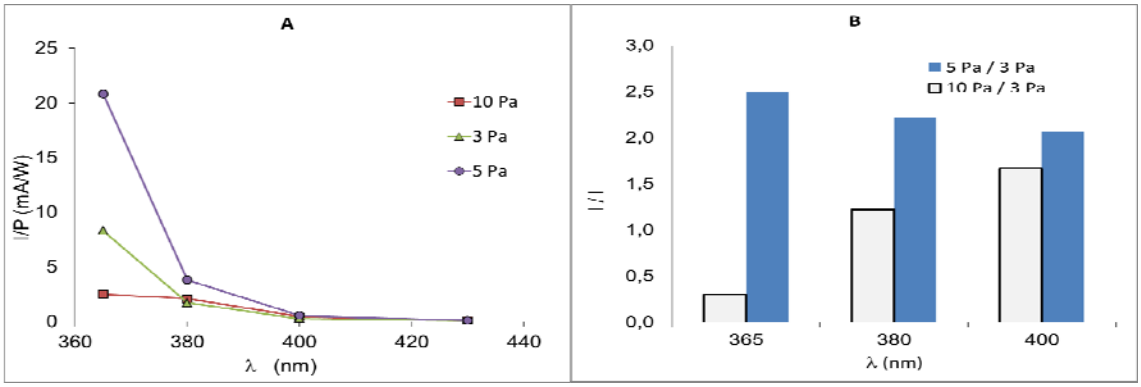

Figure 2: (A) Values of photocurrent, normalized with respect to the power of incident light, obtained at different wavelengths on samples prepared varying the oxygen partial pressure. Applied overpotential 0.5V. (B) Ratio between the photocurrents measured for the samples deposited at 5 or 10Pa and photocurrents measured for the sample deposited at 3Pa.

Moreover, the best performances are associated with the sample prepared at 5Pa: this is particularly evident for the lower wavelengths (365 and 380 nm), whereas no appreciable differences are noticeable at the higher investigated wavelengths (400 and 430 nm) because of the low absolute values of the currents measured. However, further considerations can be derived from Figure 2B where the same results are shown in terms of the ratio between the photocurrents measured for the samples deposited at 5 or 10Pa and the photocurrents measured for the sample deposited at 3Pa. As expected, under UV conditions (at 365 and 380 nm) the best performances are obtained for the sample deposited at 5Pa. However, at higher investigated wavelengths the sample deposited at 10Pa gains in efficiency compared to the other samples: in particular, moving from 365 to 400 nm, its performance exceeds that of the sample deposited at 3Pa and becomes comparable to that of the sample deposited at 5Pa.

The capacitive performance of samples was investigated using the CV and EIS techniques.
Figure 3 shows capacitance values estimated through CV measurements carried out in the dark, in a potential window from -0.1 to 0 V, where typical rectangular shapes of CV were obtained indicating capacitive behaviour of the samples. Data in Figure 3A and 3B were derived with low (10 mVs^{-1}) and high (100 mVs^{-1}) scan rates, respectively. As it clearly appears, the maximum capacitance is measured at low scan rate. This is not surprising, since under these conditions the global capacitance is determined, which can be correlated to the electrochemical response of the whole oxide films, under near-equilibrium conditions: both slow and fast responsive sites may be involved in the measurement. Otherwise, the capacitance measured with high scan rate likely originates by the response of only the outer part of the films surface (the fast responsive sites), i.e. named external capacitance. It is noticed that the highest value of global capacitance is obtained for sample deposited at 10Pa; however, being the external capacitance for this sample comparable to those measured for the samples deposited at 3 and 5Pa, it can

be deduced that most of the capacitance in the 10Pa sample is associated with microporosity. Accordingly, as shown in Figure 3C, the lowest value for the ratios of external to global capacitance is apparent for this sample.

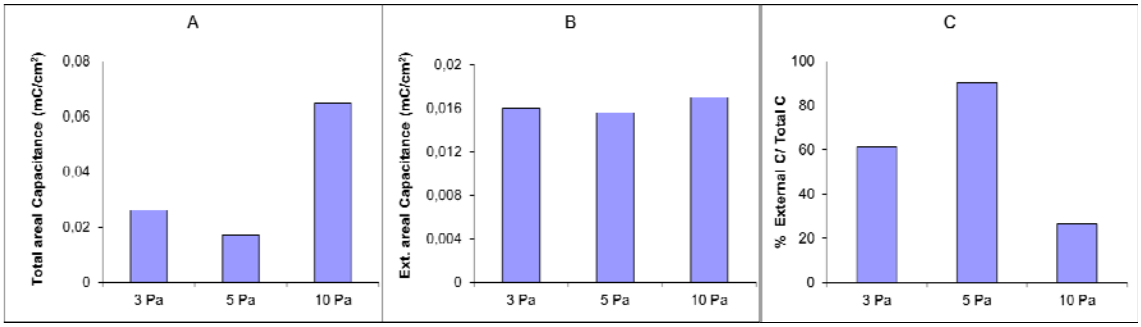

Figure 3: Values of capacitance derived from CV measurements at low (A) and high scan rate (B) in the dark. Percentage of estimated external capacitance (C).

Impedance measurements in the dark were also performed to gain further information on samples capacitance. In particular, the measurements were done at a potential value of 0.4V where all the samples showed a capacitive behavior. Figure 4 shows the results in terms of C modulus vs f, the real and imaginary components of the complex capacitance calculated as follows:

$$C'(\omega) = \frac{-Z''(\omega)}{\omega|Z(\omega)|^2} \qquad 1) \qquad\qquad C''(\omega) = \frac{Z'(\omega)}{\omega|Z(\omega)|^2} \qquad 2)$$

where Z'(ω) and Z''(ω) are the real and imaginary parts of the complex impedance Z(ω), respectively, and ω is the angular frequency ω=2πf.
At high frequencies, where charge storage at the exterior surface of the electrode dominates, all the samples show similar capacitance behavior. Differences are instead observed at the lowest frequencies, which should reflect also the contribution of bulk sites. In line with the results from CV, also EIS data reveal that the highest capacitance performance is apparent for the sample deposited at 10Pa and also in this case, the most important differences in the capacitance values are obtained at the lowest frequencies, where microporosity dominates.

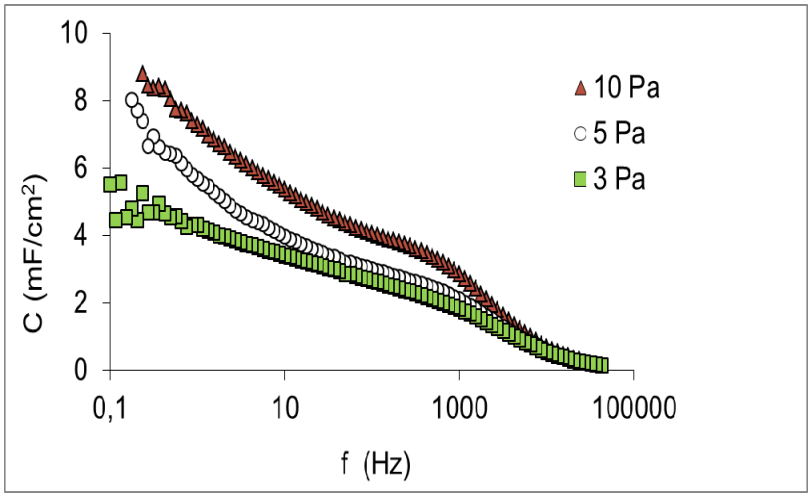

Figure 4: EIS measurements under dark conditions at 0.4V in KOH: effect of the frequency on samples capacitance.

CV measurements were also performed in a wide range of potential in order to provide useful information on both quantity and accessibility of the existing active sites.

As an example, Figure 5 shows the comparison between the CVs obtained with a scan rate of 200 mVs^{-1} for the samples deposited at 5Pa and 10Pa, which gave the highest and lowest photocurrent (see figure 2A), respectively. As it can be observed, for both samples a reduction peak is evident around −0.9 V, which can be attributed to quasi-reversible redox Ti^{+4}/Ti^{+3} couple (Beermann et al., 2002; Palmas et al., 2012). Of note, negative currents start to increase at less cathodic potential at sample deposited at 10Pa, indicating a less polarized surface. However, the lower current measured at the cathodic peak for this sample suggests a lower amount of active sites, in comparison to the sample deposited at 5Pa. This may be one of the reasons for the lower photocurrent obtained at this sample in the UV range.

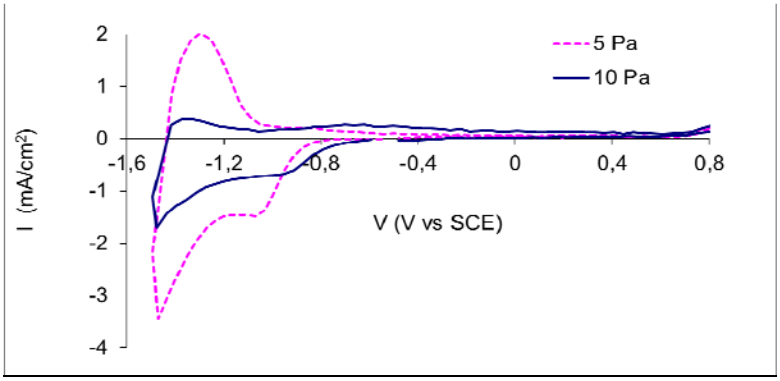

Figure 5: Comparison between voltammetric scans performed in 0.1 M KOH with a scan rate of 200 mVs^{-1} *in the dark. OCV: -0.47V (5Pa); -0.51V (10Pa).*

Data presented above highlight a complex behavior of the samples, depending on both O_2 pressure, and wavelength of the incident light.

If the effect of pressure is considered, the best photocurrent behaviour found for the sample deposited at 5Pa can be attributed to a balance between available surface area and electron transport/recombination related to the crystallinity and connectivity of the structure. In fact, an increase in the deposition pressure corresponds to an increase in porosity and in the available active surface area (as discussed in (Passoni et al., 2013)). Thus, the sample deposited at 5Pa O_2, for which a specific surface area of about 23 m^2/g was measured by BET analysis, shows a better photoactivity than the compact sample at 3Pa. However, as deposition pressure is increased up to 10Pa, porosity and thus film thickness increase, and this could negatively affect electrical transport as a consequence of the excessive length of the electron path and increased recombination losses related to the more open structure and smaller connectivity between nanoparticles.

If the effect of the different wavelength is considered, the behaviour of the samples may be justified taking into account that the lower the wavelength, the higher its energy; at the same time, the absorption coefficient of the light increases as the wavelength decreases, and in turn a lower penetration path of the radiation is obtained at the lowest wavelength (Palmas et al., 2013). In this contest, a second effect of the pressure may be considered: at the highest pressure, higher concentration of active sites could be originated at deeper energetic levels which may be involved in the process only by the most penetrating wavelengths, thus explaining the best performance of this sample at 400 nm. Also, small differences in the optical bandgap may be originated from the different defectivity, but further investigation is needed to confirm this hypothesis.

4. Conclusions

The photo electrochemical performances of hierarchically grown titanium oxide films were investigated in this work. Depending on the different morphology/structure of the TiO_2 anodes, the photocurrent responses were found to change as a function of both the O_2 pressure used in the synthesis and the irradiated wavelength.

The best performance in the UV range was obtained at the sample prepared at 5 Pa O_2 pressure; the highest external capacitance, as well as a high concentration of superficial sites evidenced by the CV, are in agreement with this result. An increase in the pressure leads to higher internal surface, but also a different distribution of active sites. Thus, on the sample prepared at 10Pa a higher concentration of

deeper energetic levels may be involved in the process when the most penetrating wavelength (400nm) is used.

References

Di Fonzo F., Casari C.S., Russo V., Brunella M.F., Li Bassi A., Bottani C.E., 2009, Hierarchically organized nanostructured TiO_2 for photocatalysis applications, Nanotechnology 20, 015604.

Beermann N., Boschloo G.K., Hagfeldt A., 2002, Trapping of electrons in nanostructured TiO_2 studied by photocurrent transients, Journal of Photochemistry and Photobiology A: Chemistry 152, 213-218.

Palmas S., Da Pozzo A., Mascia M., Vacca A., Ricci P.C., Matarrese R., 2012, On the redox behaviour of glycerol at TiO_2 electrodes, Journal of Solid State Electrochemistry 16, 2493-2502.

Passoni L., Ghods F., Docampo P., Abrusci A., Martí-Rujas J., Ghidelli M., Divitini G., Ducati C., Binda M., Guarnera S., Li Bassi A., Casari C.S., Snaith H.J., Petrozza A., Di Fonzo F., 2013, Hyperbranched Quasi-1D Nanostructures for Solid-State Dye-Sensitized Solar Cells, ACS Nano 7, 10023-10031.

Palmas S., Mascia M., Vacca A., Tredici I., 2013, Photoelectrocatalytic performances of nanostructured/decorated TiO_2 electrodes: effect of wavelength and cell configuration. Int. J. of Photoenergy, vol2013 article ID 173760 http://dx.doi.org/10.1155/2013/173760

Sauvage F., Di Fonzo F., Li Bassi A., Casari C.S., Russo V., Divitini G., Ducati C., Bottani C.E., Comte P., Graetzel M., 2010, Hierarchical TiO_2 photo-anode for dye-sensitized solar cells, NanoLetters 10, 2562-2567.